

Avoiding Membrane Locking with Regge Interpolation

Michael Neunteufel^{a,1}, Joachim Schöberl^a

^a Institute for Analysis and Scientific Computing, TU Wien, Wiedner Hauptstraße 8-10, 1040 Wien, Austria

Abstract

In this paper a novel method to overcome membrane locking of thin shells is presented. An interpolation operator into the so-called Regge finite element space is inserted in the membrane energy term to weaken the implicitly given kernel constraints. Due to the tangential-tangential continuity of Regge elements, the number of constraints is asymptotically halved on triangular meshes compared to reduced integration techniques. Provided the interpolant, this approach can be incorporated easily to any shell element. The performance of the proposed method is demonstrated by means of several benchmark examples.

Keywords: locking, shells, finite elements, Regge calculus

1 Introduction

In mathematical formulations of plates and shells a small parameter, the thickness, is involved. The lack of finite element approximations of the hidden constraints of the physical model leads to so-called locking phenomena [4, 13]. For shells shear and membrane locking can be observed. The shear locking, induced by the Kirchhoff constraint in the limit case, has been extensively discussed and a variety of shear locking free plate and shell elements have been proposed [5, 9, 28]. For membrane locking, also called inextensional locking, where the (curved) elements fail to represent pure bending, only little analysis

has been done [1, 23, 19, 14] and mostly reduced integration schemes are used in practice [43, 36, 37]. There, the membrane constraints are weakened due to under-integration. It is well known that (sufficient high) p and hp-refinement strategies [29, 38, 20] can overcome the problem of membrane locking, but in the case of low order triangular elements the reduced integration techniques suffer [14].

Tullio Regge derived in [32] a geometric discretization of the Einstein field equations by approximations with a piece-wise constant metric. In theoretical, and later also numerical, physics, so-called Regge calculus was applied e.g., in fields of relativity and quantum mechanics and has been further developed the last fifty years, see [40] for an overview. An analytical point of view of Regge calculus were given in [12, 11]. It was observed that Regge's approach is equivalent to specify lengths at all edges of a mesh, similar to Whitney-forms [39]. In the context of finite element exterior calculus (FEEC) [3, 2] a finite element point of view were given in [15, 16] and the resulting Regge elements have been generalized to arbitrary polynomial order on triangles and tetrahedrons [24].

In this work we will use the resulting Regge interpolant to construct membrane locking free methods for shells. It can be incorporated in any existing method and finite element code, providing the interpolation operator. In a variety of numerical examples the method is tested.

This paper is structured as follows: In the next section we will give a brief overview of Regge elements and the according interpolation operator. Then the method is described in the general case of shells. In section 4 the method is discussed. In the last section we apply the resulting method to several established membrane locking benchmark examples.

2 Regge elements

For the convenience of the reader we give a brief introduction in the construction of Regge elements. As the Regge elements approximate symmetric tensors we seek for a matrix valued finite element space. To prescribe the edge lengths globally only the tangential-tangential components need to be globally continu-

¹Corresponding author.

E-mail address: michael.neunteufel@tuwien.ac.at

ous. Therefore, let \mathcal{T}_h a triangulation of a domain $\Omega \subset \mathbb{R}^d$. The set of all piece-wise polynomials up to degree k on \mathcal{T}_h is denoted by $\Pi^k(\mathcal{T}_h)$. With this, we define the Regge finite element space

$$\text{Reg}^k := \{\boldsymbol{\sigma} \in [\Pi^k(\mathcal{T}_h)]_{\text{sym}}^{d \times d} : \llbracket \boldsymbol{\sigma}_{tt} \rrbracket = 0\}, \quad (2.1)$$

where $\boldsymbol{\sigma}_{tt}$ is the tangential-tangential component in two or the 2×2 tangential-tangential sub-matrix in three dimensions and $\llbracket \boldsymbol{\sigma}_{tt} \rrbracket$ denotes the tangential-tangential jump over elements.

Further, we define the Lagrangian nodal finite element space as

$$V_h^k := \Pi^k(\mathcal{T}_h) \cap C^0(\Omega), \quad (2.2)$$

where $C^0(\Omega)$ denotes to set of all continuous functions on Ω . For an (high-order) construction of H^1 -conforming finite elements we refer to [7, 42, 41].

In the context of [22] we can define functionals, the degrees of freedom (dofs), on the reference or physical tetrahedron T with the local space $[\Pi^k(T)]_{\text{sym}}^{3 \times 3}$. Therefore, let $\{q_{E,l}\}$, $\{q_{F,l}\}$ and $\{q_{T,l}\}$ denote a basis of $\Pi^k(E_{\alpha\beta})$ on the edge $E_{\alpha\beta}$ between to vertices $\alpha \neq \beta$, $[\Pi^{k-1}(F_\alpha)]_{\text{sym}}^{3 \times 3}$ on the face F_α $\alpha = 1, \dots, 4$ and $[\Pi^{k-2}(T)]_{\text{sym}}^{3 \times 3}$ on the tetrahedron T , respectively. Then the functionals read

$$\Psi_{E_{\alpha\beta},l} : \boldsymbol{\sigma} \mapsto \int_{E_{\alpha\beta}} \boldsymbol{\sigma} : q_{E,l} t_E \otimes t_E d\lambda_1, \quad (2.3)$$

$$\Psi_{F_\alpha,l} : \boldsymbol{\sigma} \mapsto \int_{F_\alpha} \boldsymbol{\sigma} : \mathbf{q}_{F,l} d\lambda_2, \quad (2.4)$$

$$\Psi_{T,l} : \boldsymbol{\sigma} \mapsto \int_T \boldsymbol{\sigma} : \mathbf{q}_{T,l} d\lambda_3, \quad (2.5)$$

where $\mathbf{A} : \mathbf{B} := \sum_{ij} \mathbf{A}_{ij} \mathbf{B}_{ij}$ denotes the Frobenius scalar product, \otimes the outer dyadic product and t_E the tangent vector of the edge $E_{\alpha\beta}$. For triangles the functionals are defined analogously.

In one dimension the Regge elements coincide with L^2 -conforming discontinuous finite elements. On two-dimensional triangular elements they are equivalent to the $H(\text{divdiv})$ finite elements constructed in [35]. Like the relationship between $H(\text{div})$ [31, 8] and $H(\text{curl})$ [25, 26] elements in 2D, one has to rotate the shape functions. In three dimensions, however, these

spaces differ as the Regge elements have more coupling degrees of freedom, see Figure 2.1 for the lowest order and first order Regge elements on segments, triangles and tetrahedrons.

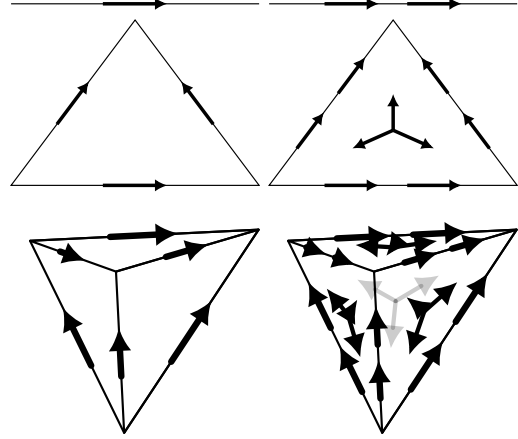


Figure 2.1: Lowest order and first order Regge elements for segments, triangles and tetrahedrons.

An explicit basis for the according shape functions $\{\varphi_i\}$ to (2.3)-(2.5) is constructed e.g., in [24]. Given these functionals $\{\Psi_i\}$ and shape functions $\{\varphi_i\}$, one can define the following Regge interpolation operator

$$\begin{aligned} \mathcal{I}_{h,k}^R : [C^\infty(\Omega)]_{\text{sym}}^{d \times d} &\rightarrow \text{Reg}^k \\ \boldsymbol{\sigma} &\mapsto \sum_{i=0}^{N_k} \Psi_i(\boldsymbol{\sigma}) \varphi_i, \end{aligned} \quad (2.6)$$

where $N_k \in \mathbb{N}$ denotes the number of degrees of freedom (the number of shape functions) and $C^\infty(\Omega)$ the set of all smooth functions on Ω .

If a Regge element $\hat{\boldsymbol{\sigma}}_h$ is defined on the reference tetrahedron or triangle \hat{T} , one needs to map it to a physical element $T = \Phi(\hat{T})$, given by a transformation $\Phi : \hat{T} \rightarrow \mathbb{R}^d$, in such a way that the tangential-tangential continuity gets preserved. For $H(\text{curl})$ -conforming elements the covariant transformation $u \circ \Phi := \mathbf{F}^{-T} \hat{u}$, $\mathbf{F} := \nabla \Phi$, is used to preserve the tangential continuity. Thus, by applying the co-

variant transformation on both sides,

$$\boldsymbol{\sigma}_h \circ \Phi := \mathbf{F}^{-T} \hat{\boldsymbol{\sigma}}_h \mathbf{F}^{-1} \quad (2.7)$$

leads to a symmetric tangential-tangential continuous function $\boldsymbol{\sigma}_h$ on T . For shells one needs to map the reference triangle $\hat{T} \subset \mathbb{R}^2$ to a (possibly curved) surface triangle $T \subset \mathbb{R}^3$. The deformation gradient $\mathbf{F} \in C^\infty(\Omega, \mathbb{R}^{3 \times 2})$ is not invertible and thus, the transformation rule (2.7) needs to be adopted by using the Moore–Penrose pseudo-inverse instead

$$\boldsymbol{\sigma}_h \circ \Phi := (\mathbf{F}^\dagger)^T \hat{\boldsymbol{\sigma}}_h \mathbf{F}^\dagger. \quad (2.8)$$

3 Methodology

3.1 Shells and membrane energy

Let $\hat{\Omega} \subset \mathbb{R}^3$ be an undeformed configuration of a shell with thickness t , described by the mid-surface S and the according orientated normal vector ν_S

$$\Omega := \{\hat{x} + z\nu_S(\hat{x}) : \hat{x} \in S, z \in [-t/2, t/2]\}. \quad (3.1)$$

Furthermore, let $\Phi : \Omega \rightarrow \mathbb{R}^3$ be the deformation from the initial to the deformed configuration of the shell and $\phi : S_h \rightarrow \mathbb{R}^3$ the deformation of the approximated mid-surface. The according triangulation consisting of possibly curved triangles of S_h is denoted by \mathcal{T}_h . Then, we define $\mathbf{F} := \nabla_\tau \phi$ as the deformation gradient. Here, $\nabla_\tau \phi$ denotes the surface gradient of ϕ , which can be introduced in weak sense [18], or directly as Fréchet-derivative. We can split the deformation into the identity function and the displacement, $\phi = \text{id} + u$, and thus, $\mathbf{F} = \mathbf{P}_\tau + \nabla_\tau u$ with the projection onto the tangent plane $\mathbf{P}_\tau := \mathbf{I} - \nu \otimes \nu$.

The shell energy functional can be split into a membrane, bending and shear energy part, cf. [17, 10, 6],

$$\mathcal{W}(u) = \frac{t}{2} E_{\text{mem}} + \frac{t^3}{2} E_{\text{bend}} + \frac{t}{2} E_{\text{shear}} - f(u), \quad (3.2)$$

where f denotes an external force.

We focus on the membrane energy and consider the full nonlinear term

$$E_{\text{mem}} := \int_S \|\mathbf{E}_\tau\|_{\mathbf{M}}^2 dx, \quad (3.3)$$

with $\mathbf{E}_\tau := 1/2(\mathbf{C}_\tau - \mathbf{I})$ denoting the Green strain tensor restricted on the tangent plane, $\mathbf{C}_\tau := \mathbf{F}^T \mathbf{F}$ denoting the Cauchy–Green strain tensor. The material norm is given by

$$\|\cdot\|_{\mathbf{M}}^2 := \frac{E}{1-\nu^2} (\nu \text{tr}(\cdot)^2 + (1-\nu) \text{tr}(\cdot^2)), \quad (3.4)$$

with the material tensor \mathbf{M} , the Young’s modulus E and the Poisson’s ratio ν , respectively.

The linearization of (3.3) is given by

$$\begin{aligned} E_{\text{mem}}^{\text{lin}} &:= \int_S \|\text{sym}(\mathbf{P}_\tau \nabla_\tau u)\|_{\mathbf{M}}^2 dx \\ (E_{\text{mem}}^{\text{lin}})_{\alpha\beta} &= \int_S \left\| \frac{1}{2}(u_{\alpha|\beta} + u_{\beta|\alpha}) - b_{\alpha\beta} u_3 \right\|_{\mathbf{M}}^2 dx, \end{aligned} \quad (3.5)$$

where $u_{\alpha|\beta}$ denotes the covariant derivative, $b_{\alpha\beta}$ the second fundamental form, $\alpha, \beta \in \{1, 2\}$, and u_3 the displacement components in normal direction, see e.g. [10] for the notations.

3.2 Usage of Regge interpolant

In what follows let the discrete displacements $u_h \in [V_h^k]^3$. For our proposed method we insert the Regge interpolation operator of order $k-1$ into the membrane energy (3.3)

$$\int_S \frac{t}{2} \|\mathcal{I}_{h,k-1}^R \mathbf{E}_\tau\|_{\mathbf{M}}^2 dx, \quad (3.6)$$

which is equivalent to introduce a Lagrange functional \mathcal{L} and two new unknowns $\mathbf{R} \in \text{Reg}^{k-1}$ and $\mathbf{Q} \in [\text{Reg}^{k-1}]^*$ and using the following terms instead of (3.6)

$$\int_S \frac{t}{2} \|\mathbf{R}\|_{\mathbf{M}}^2 dx + \langle \mathbf{Q}, \mathbf{R} - \mathbf{E}_\tau \rangle. \quad (3.7)$$

Here, $[\text{Reg}^k]^*$ denotes the discrete dual space of Regge elements consisting of the functionals (2.3)-(2.5) and

$$\begin{aligned} \langle \cdot, \cdot \rangle : [\text{Reg}^k]^* \times \text{Reg}^k &\rightarrow \mathbb{R}, \\ (\Psi, \varphi) &\mapsto \Psi(\varphi), \end{aligned} \quad (3.8)$$

denoting the canonical pairing.

With this, the new Lagrange functional reads

$$\begin{aligned} \mathcal{L}(u, \mathbf{R}, \mathbf{Q}) &= \int_S \frac{t}{2} \|\mathbf{R}\|_M^2 dx + \langle \mathbf{Q}, \mathbf{R} - \mathbf{E}_\tau \rangle \\ &\quad + \frac{t^3}{2} E_{\text{bend}} + \frac{t}{2} E_{\text{shear}}. \end{aligned} \quad (3.9)$$

Due to the tangential-tangential continuity of \mathbf{E}_τ , the discrete Jacobean $\nabla_\tau u_h$ is tangential-continuous, it is mathematically equivalent to break the continuity of Reg^k and its dual space $[\text{Reg}^k]^*$ and apply the projection element-wise. Hence, static condensation techniques can be applied to eliminate the two unknowns \mathbf{R} and \mathbf{Q} locally. This makes the method cheap and positive definite systems get preserved.

4 Discussion

Let u be an exact solution to the shell problem (3.2) such that $E_{\text{mem}}^{\text{lin}}(u) = 0$. Interpolating u into the Lagrangian finite element space $[V_h^k]^3$, $u_h := \mathcal{I}_{h,k} u$, \mathcal{I}_h denoting the standard nodal interpolation operator, does not guarantee in general that $E_{\text{mem}}^{\text{lin}}(u_h) = 0$ for the discrete displacements. I.e. the interpolation operator does not preserve the kernel of the membrane operator. Therefore, pure bending modes induce discrete membrane energy modes due to the discrete constraints. This effect dominates for small thickness parameter t , the shell element is called to be too stiff and locking occurs.

By using the Regge interpolant $\mathcal{I}_{h,k-1}^R E_{\text{mem}}^{\text{lin}}(u_h)$ we weaken the discrete constraints. Reduced integration schemes follow the same idea, using less Gauß-integration points, which corresponds to an L^2 -interpolation instead of a Regge interpolation. When we compare the number of dofs, which can be interpreted as the number of constraints, one can observe that on one single triangle T the number of

constraints are equal as the dimension of both spaces are the same, $\dim = 3(k+1)(k+2)/2$.

For a triangulation \mathcal{T}_h , however, the number of constraints differ already in the lowest order case significantly. For Regge elements we have one degree of freedom per edge, whereas in the reduced integration scheme one has three per element. Asymptotically there holds

$$\#T \approx 2\#V, \quad \#E \approx 3\#V, \quad (4.1)$$

where $\#T$, $\#E$, and $\#V$ denote the number of triangles, edges, and vertices of the triangulation \mathcal{T}_h . Therefore,

$$\#E \approx 3\#V < 6\#V \approx 3\#T \quad (4.2)$$

and thus, the Regge interpolation reduces the number of constraints asymptotically by a factor of two compared to the L^2 -projection. Furthermore, on a triangulation \mathcal{T}_h of a flat two-dimensional domain or a surface described by one single embedding (and thus not closed) there holds

$$3 + \#E = 3\#V - \#V_B = 2\#V + \#V_I, \quad (4.3)$$

where $\#V_B$ and $\#V_I$ denote the number of vertices on the boundary and in the inner domain, respectively. The discrepancy of three corresponds to the number of rigid-body motions in two dimensions, two translations and one rotation. Therefore, for given displacements at the vertices one can find a unique value per edge describing the (tangential-tangential) stretching between two vertices. This fits perfectly to the following (linear) exact sequence

$$\begin{array}{ccc} RB & \xrightarrow{\text{id}} & [C^\infty(\Omega)]^2 \xrightarrow{\nabla_{\text{sym}}} [C^\infty(\Omega)]_{\text{sym}}^{2 \times 2} \\ & & \mathcal{I}_h \downarrow \qquad \qquad \mathcal{I}_h^R \downarrow \\ RB & \xrightarrow{\text{id}} & [V_h^k]^2 \xrightarrow{\nabla_{\text{sym}}} \text{Reg}^{k-1} \end{array}, \quad (4.4)$$

where $RB := \{Ax + b \mid A \in \mathbb{R}^{2 \times 2}, A^T = -A, b \in \mathbb{R}^2\}$ denotes the set of linearized rigid body motions.

In [16, 21] they used this sequence in three dimensions as a part of a larger complex and proofed in the lowest order case commuting and exactness properties. For a nonlinear complex one has to replace the

symmetric gradient by the Green strain tensor and $RB = \{Ax + b \mid A \in SO(2), b \in \mathbb{R}^2\}$, where $SO(2)$ denotes the set of all orthogonal 2×2 matrices with determinant one.

In the case of the full nonlinear membrane energy term (3.3) the Green strain operator $\mathbf{E}_\tau : [\Pi^k(\mathcal{T}_h)]^d \rightarrow [\Pi^{2k-2}(\mathcal{T}_h)]_{\text{sym}}^{d \times d}$ doubles the polynomial degree asymptotically element-wise, with the exception $k = 1$. This may lead to even worse discrete kernel conservation. Thanks to the Regge interpolant, the Green strain tensor gets projected back to polynomial degree $k - 1$ and again the number of constraints are reduced.

In the lowest order case $k = 1$ for the displacements, membrane locking is not observed as long as an isoperimetric mapping for the shell geometry is considered. Curving the geometry by a higher polynomial degree as the displacements leads to enormous membrane locking in the lowest order case. However, using the Regge interpolation $\mathcal{I}_{h,0}^R$ reduces this locking phenomena too.

5 Numerical examples

To avoid shear locking effects we use the Kirchhoff-Love shell model introduced in [27]. The method is implemented in the NGS-Py interface, which is based on the finite element library Netgen/NGSolve² [33, 34]. As the discrete dual space $[\text{Reg}^k]^*$ is implemented in NGSolve, method (3.9) can be used directly.

For the benchmarks we use lowest order element, i.e. polynomial order $k = 1$ for the displacements, together with quadratically curved meshes, which will be denoted by method p1. Further, second order finite elements for the displacements, where the geometry is mapped isoperimetrically, i.e. also quadratic elements, are used, called method p2.

The forces are chosen such that the deformations are in the linear regime. Therefore, the differences between the linearized (3.5) and full nonlinear (3.3) membrane energy is marginal. Further, the forces are scaled appropriately with the thickness parameter t

²www.ngsolve.org

such that the deformations are in the same magnitude. Due to the nonlinear bending energy part in [27], however, the results may vary with respect to the thickness parameter. The reference values are computed by a very fine mesh and the error is computed by $|results - reference|/reference$.

5.1 Cylinder with free ends

A cylinder with free ends is loaded with a periodic force [30, 10], see Figure 5.1. By symmetries the computational domain is one eighth of the original and symmetry boundary conditions are used, see Figure 5.2. The material and geometric parameters are $R = 1$, $E = 3 \times 10^4$, $\nu = 0.3$, $t \in \{0.1, 0.01, 0.001, 0.0001\}$ and the cylinder is loaded by the normal pressure distribution $P = t^3 \cos(2\zeta)\hat{\nu}$, ζ and $\hat{\nu}$ denoting the circumferential arc-length and the normal vector on the reference configuration, respectively, cf. Figure 5.1.

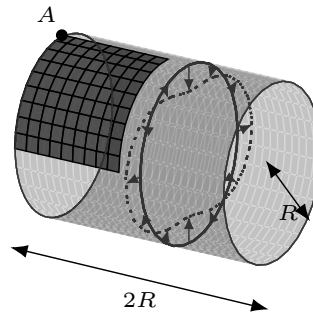


Figure 5.1: Geometry for Cylinder with free ends benchmark.

The radial deflection at point A is measured and listed in Table 5.1 - 5.4 and the relative error can be found in Figure 5.3 and 5.4.

5.2 Axisymmetric hyperboloid with free ends

An axisymmetric hyperboloid is described by the equation

$$x^2 + y^2 = R^2 + z^2, \quad z \in [-R, R] \quad (5.1)$$

	1e-01	1e-02	1e-03	1e-04
10	-2.46e-05	-5.18e-07	-5.26e-09	-5.26e-11
38	-3.58e-05	-1.38e-06	-1.44e-08	-1.44e-10
160	-4.33e-05	-5.02e-06	-5.57e-08	-5.57e-10
644	-4.54e-05	-1.64e-05	-2.57e-07	-2.60e-09
2592	-4.59e-05	-3.18e-05	-1.07e-06	-1.10e-08
10368	-4.60e-05	-4.07e-05	-4.07e-06	-4.51e-08
41552	-4.60e-05	-4.36e-05	-1.27e-05	-1.79e-07

Table 5.1: Results for cylinder with free ends, method p1 without Regge interpolation.

	1e-01	1e-02	1e-03	1e-04
10	-5.36e-05	-5.07e-05	-5.06e-05	-5.06e-05
38	-4.77e-05	-4.24e-05	-4.04e-05	-4.04e-05
160	-4.67e-05	-4.50e-05	-4.33e-05	-4.29e-05
644	-4.62e-05	-4.48e-05	-4.45e-05	-4.38e-05
2592	-4.61e-05	-4.47e-05	-4.45e-05	-4.44e-05
10368	-4.61e-05	-4.47e-05	-4.45e-05	-4.44e-05
41552	-4.60e-05	-4.47e-05	-4.45e-05	-4.45e-05

Table 5.2: Results for cylinder with free ends, method p1 with Regge interpolation.

	1e-01	1e-02	1e-03	1e-04
10	-2.87e-05	-1.47e-05	-1.39e-05	-1.34e-05
38	-4.21e-05	-1.99e-05	-7.43e-06	-6.84e-06
160	-4.58e-05	-3.44e-05	-1.52e-05	-3.73e-06
644	-4.60e-05	-4.37e-05	-2.65e-05	-8.88e-06
2592	-4.60e-05	-4.47e-05	-3.96e-05	-2.02e-05
10368	-4.60e-05	-4.47e-05	-4.41e-05	-3.03e-05
41552	-4.60e-05	-4.47e-05	-4.45e-05	-4.21e-05

Table 5.3: Results for cylinder with free ends, method p2 without Regge interpolation.

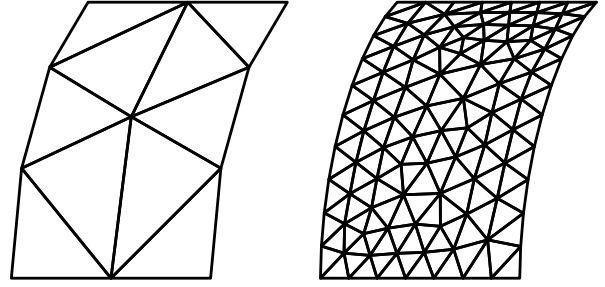


Figure 5.2: Uncurved meshes with 10 and 162 elements for Cylinder with free ends benchmark.

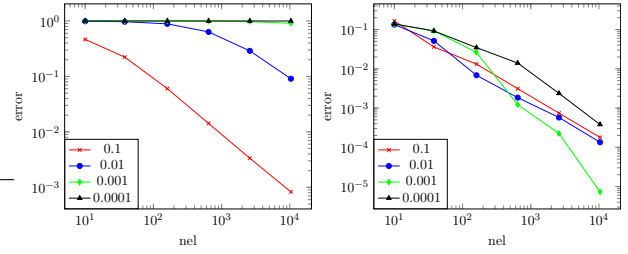


Figure 5.3: Results for cylinder with free ends, method p1 without and with Regge interpolation.

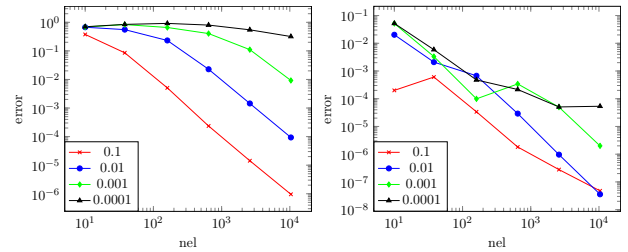


Figure 5.4: Results for cylinder with free ends, method p2 without and with Regge interpolation.

with free boundaries is loaded by a force, see [10]. Due to symmetries it is sufficient to use one eighth of the geometry and symmetry boundary conditions, see Figure 5.5 for the geometry and Figure 5.6 for a coarse and fine mesh. The material and geometric parameters are $R = 1$, $E = 2.85 \times 10^4$, $\nu = 0.3$, $t \in$

$$\{0.1, 0.01, 0.001, 0.0001\}, P = \frac{t^3}{\sqrt{x^2+y^2}} \cos(2\zeta) \begin{pmatrix} x \\ y \\ 0 \end{pmatrix}$$

	1e-01	1e-02	1e-03	1e-04
10	-4.61e-05	-4.38e-05	-4.22e-05	-4.21e-05
38	-4.60e-05	-4.46e-05	-4.44e-05	-4.42e-05
160	-4.60e-05	-4.47e-05	-4.45e-05	-4.45e-05
644	-4.60e-05	-4.47e-05	-4.45e-05	-4.45e-05
2592	-4.60e-05	-4.47e-05	-4.45e-05	-4.45e-05
10368	-4.60e-05	-4.47e-05	-4.45e-05	-4.45e-05
41552	-4.60e-05	-4.47e-05	-4.45e-05	-4.45e-05

Table 5.4: Results for cylinder with free ends, method p2 with Regge interpolation.

similar to the previous benchmark.

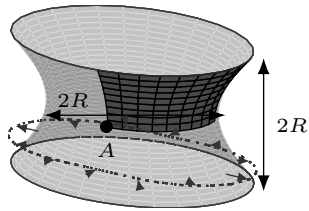


Figure 5.5: Geometry for Axisymmetric hyperboloid with free ends benchmark.

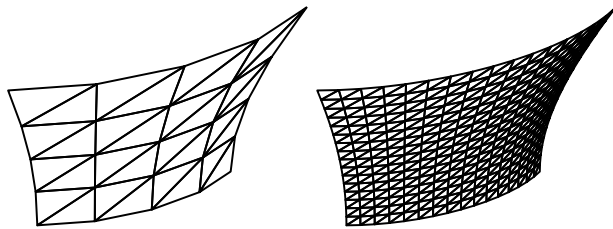


Figure 5.6: Uncurved meshes with 32 and 512 elements for Axisymmetric hyperboloid with free ends benchmark.

The radial deflection at point A is can be found in Table 5.5 - 5.8 and the relative error in Figure 5.7 and 5.8.

	1e-01	1e-02	1e-03	1e-04
8	-6.66e-06	-8.79e-08	-8.83e-10	-8.83e-12
32	-1.24e-05	-2.55e-07	-2.59e-09	-2.59e-11
128	-1.83e-05	-8.80e-07	-9.38e-09	-9.39e-11
512	-2.12e-05	-2.89e-06	-3.53e-08	-3.54e-10
968	-2.18e-05	-4.72e-06	-6.55e-08	-6.59e-10
2048	-2.22e-05	-7.72e-06	-1.36e-07	-1.38e-09
8192	-2.24e-05	-1.38e-05	-5.21e-07	-5.42e-09
32768	-2.25e-05	-1.73e-05	-1.89e-06	-2.15e-08

Table 5.5: Results for axisymmetric hyperboloid with free ends, method p1 without Regge interpolation.

	1e-01	1e-02	1e-03	1e-04
8	-4.28e-05	-4.09e-05	-4.09e-05	-4.09e-05
32	-2.60e-05	-2.32e-05	-2.32e-05	-2.32e-05
128	-2.32e-05	-2.00e-05	-1.99e-05	-1.99e-05
512	-2.27e-05	-1.92e-05	-1.92e-05	-1.92e-05
968	-2.26e-05	-1.91e-05	-1.91e-05	-1.91e-05
2048	-2.25e-05	-1.90e-05	-1.90e-05	-1.90e-05
8192	-2.25e-05	-1.90e-05	-1.89e-05	-1.89e-05
32768	-2.25e-05	-1.90e-05	-1.89e-05	-1.89e-05

Table 5.6: Results for axisymmetric hyperboloid with free ends, method p1 with Regge interpolation.

	1e-01	1e-02	1e-03	1e-04
8	-1.41e-05	-8.40e-07	-2.16e-08	-2.31e-10
32	-2.00e-05	-4.10e-06	-1.23e-07	-1.28e-09
128	-2.22e-05	-1.24e-05	-1.17e-06	-1.82e-08
512	-2.25e-05	-1.77e-05	-6.12e-06	-2.54e-07
968	-2.25e-05	-1.86e-05	-1.03e-05	-7.41e-07
2048	-2.25e-05	-1.89e-05	-1.46e-05	-2.09e-06
8192	-2.25e-05	-1.90e-05	-1.84e-05	-9.15e-06
32768	-2.25e-05	-1.90e-05	-1.89e-05	-1.64e-05

Table 5.7: Results for axisymmetric hyperboloid with free ends, method p2 without Regge interpolation.

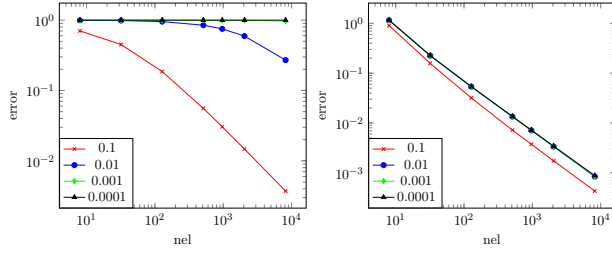


Figure 5.7: Results for axisymmetric hyperboloid with free ends, method p1 without and with Regge interpolation.

	1e-01	1e-02	1e-03	1e-04
8	-2.25e-05	-1.94e-05	-1.93e-05	-1.93e-05
32	-2.25e-05	-1.90e-05	-1.90e-05	-1.90e-05
128	-2.25e-05	-1.90e-05	-1.89e-05	-1.89e-05
512	-2.25e-05	-1.90e-05	-1.89e-05	-1.89e-05
968	-2.25e-05	-1.90e-05	-1.89e-05	-1.89e-05
2048	-2.25e-05	-1.90e-05	-1.89e-05	-1.89e-05
8192	-2.25e-05	-1.90e-05	-1.89e-05	-1.89e-05
32768	-2.25e-05	-1.90e-05	-1.89e-05	-1.89e-05

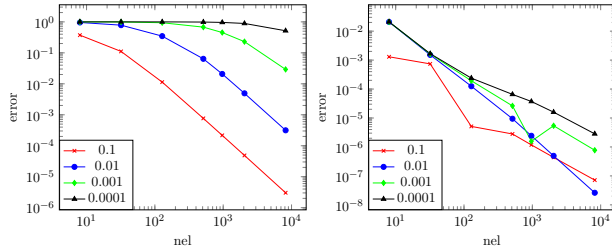


Figure 5.8: Results for axisymmetric hyperboloid with free ends, method p2 without and with Regge interpolation.

Table 5.8: Results for axisymmetric hyperboloid with free ends, method p2 with Regge interpolation.

	1e-01	1e-02	1e-03	1e-04
8	4.86e-03	6.15e-05	6.16e-07	6.16e-09
32	9.48e-03	2.09e-04	2.13e-06	2.13e-08
128	1.43e-02	7.24e-04	7.98e-06	7.99e-08
512	1.71e-02	2.21e-03	3.03e-05	3.06e-07
2048	1.80e-02	5.02e-03	1.14e-04	1.19e-06
8192	1.83e-02	7.49e-03	4.14e-04	4.62e-06
32768	1.83e-02	8.56e-03	1.36e-03	1.80e-05

5.3 Hyperbolic paraboloid

A hyperbolic paraboloid, which is described by the embedding

$$\Phi : [0, 3] \times [0, 1] \rightarrow \mathbb{R}^3$$

$$(x, y) \mapsto (x, y, \alpha(y^2 - x^2)), \quad (5.2)$$

is clamped at the bottom and subjected to a surface force f [14]. On the right side symmetry boundary conditions are used, the other boundaries are free. The material and geometric parameters are $\alpha = 0.2$, $E = 2.85 \times 10^4$, $\nu = 0.3$, $t \in \{0.1, 0.01, 0.001, 0.0001\}$, $f = 8t^3 \hat{\nu}$. Here, $\hat{\nu}$ denotes the normal vector on the reference configuration, see Figure 5.9 and 5.10.

The deflection in z-direction at point A can be seen in Table 5.9 - 5.12 and the relative error in Figure 5.11 and 5.12.

Table 5.9: Results for hyperbolic paraboloid, method p1 without Regge interpolation.

	1e-01	1e-02	1e-03	1e-04
8	2.32e-02	2.11e-02	2.11e-02	2.11e-02
32	1.77e-02	1.24e-02	1.18e-02	1.18e-02
128	1.77e-02	9.73e-03	8.47e-03	8.34e-03
512	1.82e-02	9.09e-03	7.28e-03	6.83e-03
2048	1.83e-02	9.00e-03	6.91e-03	6.25e-03
8192	1.83e-02	8.99e-03	6.83e-03	6.04e-03
32768	1.83e-02	8.99e-03	6.81e-03	5.98e-03

Table 5.10: Results for hyperbolic paraboloid, method p1 with Regge interpolation.

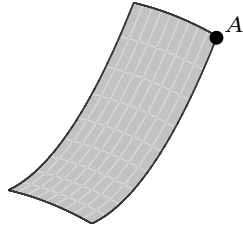


Figure 5.9: Geometry for Hyperbolic paraboloid benchmark.

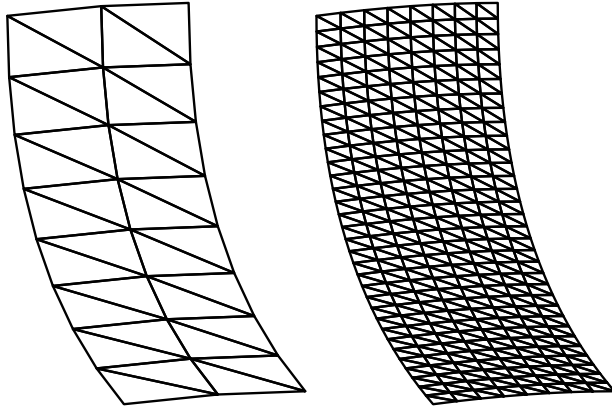


Figure 5.10: Uncurved meshes with 32 and 512 elements for Hyperbolic paraboloid benchmark.

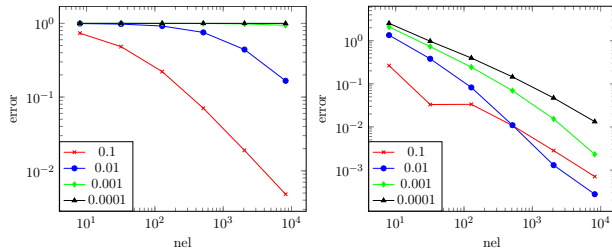


Figure 5.11: Results for hyperbolic paraboloid, method p1 without and with Regge interpolation.

Acknowledgments

Michael Neunteufel has been funded by the Austrian Science Fund (FWF) project W1245.

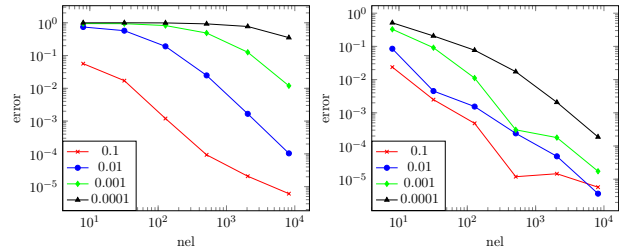


Figure 5.12: Results for hyperbolic paraboloid, method p2 without and with Regge interpolation.

	1e-01	1e-02	1e-03	1e-04
8	1.73e-02	2.31e-03	3.78e-04	2.35e-05
32	1.80e-02	3.83e-03	4.23e-04	6.34e-06
128	1.83e-02	7.27e-03	1.21e-03	6.30e-05
512	1.84e-02	8.77e-03	3.50e-03	4.45e-04
2048	1.84e-02	8.97e-03	5.95e-03	1.37e-03
8192	1.84e-02	8.99e-03	6.73e-03	3.87e-03
32768	1.84e-02	8.99e-03	6.80e-03	5.57e-03

Table 5.11: Results for hyperbolic paraboloid, method p2 without Regge interpolation.

References

- [1] ARNOLD, D., AND BREZZI, F. Locking-free finite element methods for shells. *Mathematics of Computation of the American Mathematical Society* 66, 217 (1997), 1–14.
- [2] ARNOLD, D., FALK, R., AND WINTHER, R. Finite element exterior calculus: from hodge the-

	1e-01	1e-02	1e-03	1e-04
8	1.79e-02	9.75e-03	9.04e-03	9.03e-03
32	1.84e-02	8.95e-03	7.43e-03	7.20e-03
128	1.84e-02	8.97e-03	6.89e-03	6.42e-03
512	1.84e-02	8.99e-03	6.81e-03	6.07e-03
2048	1.84e-02	8.99e-03	6.81e-03	5.98e-03
8192	1.84e-02	8.99e-03	6.81e-03	5.96e-03
32768	1.84e-02	8.99e-03	6.81e-03	5.97e-03

Table 5.12: Results for hyperbolic paraboloid, method p2 with Regge interpolation.

- ory to numerical stability. *Bulletin of the American mathematical society* 47, 2 (2010), 281–354.
- [3] ARNOLD, D. N., FALK, R. S., AND WINTHER, R. Finite element exterior calculus, homological techniques, and applications. *Acta numerica* 15 (2006), 1–155.
- [4] BABUŠKA, I., AND SURI, M. On locking and robustness in the finite element method. *SIAM Journal on Numerical Analysis* 29, 5 (1992), 1261–1293.
- [5] BATHE, K.-J., AND BREZZI, F. A simplified analysis of two plate bending elements the MITC4 and MITC9 elements. In *Numerical Techniques for Engineering Analysis and Design*. Springer, 1987, pp. 407–417.
- [6] BISCHOFF, M., BLETZINGER, K.-U., WALL, W. A., AND RAMM, E. *Models and Finite Elements for Thin-Walled Structures*. American Cancer Society, 2004, ch. 3.
- [7] BRAESS, D. *Finite Elemente - Theorie, schnelle Löser und Anwendungen in der Elastizitätstheorie*, 5 ed. Springer-Verlag, Berlin Heidelberg, 2013.
- [8] BREZZI, F., DOUGLAS, J., AND MARINI, L. D. Two families of mixed finite elements for second order elliptic problems. *Numerische Mathematik* 47, 2 (1985), 217–235.
- [9] BREZZI, F., FORTIN, M., AND STENBERG, R. Error analysis of mixed-interpolated elements for Reissner-Mindlin plates. *Mathematical Models and Methods in Applied Sciences* 1, 02 (1991), 125–151.
- [10] CHAPELLE, D., AND BATHE, K.-J. *The finite element analysis of shells - fundamentals*, 2 ed. Springer-Verlag, Berlin Heidelberg, 2011.
- [11] CHEEGER, J., MÜLLER, W., AND SCHRADER, R. On the curvature of piecewise flat spaces. *Communications in Mathematical Physics* 92, 3 (Sep 1984), 405–454.
- [12] CHEEGER, J., MÜLLER, W., AND SCHRADER, R. Kinematic and tube formulas for piecewise linear spaces. *Indiana University Mathematics Journal* 35, 4 (1 1986), 737–754.
- [13] CHENAIS, D., AND PAUMIER, J.-C. On the locking phenomenon for a class of elliptic problems. *Numerische Mathematik* 67, 4 (May 1994), 427–440.
- [14] CHOI, D., PALMA, F., SANCHEZ-PALENCIA, E., AND VILARINO, M. Membrane locking in the finite element computation of very thin elastic shells. *ESAIM: Mathematical Modelling and Numerical Analysis* 32, 2 (1998), 131–152.
- [15] CHRISTIANSEN, S. H. A characterization of second-order differential operators on finite element spaces. *Mathematical Models and Methods in Applied Sciences* 14, 12 (2004), 1881–1892.
- [16] CHRISTIANSEN, S. H. On the linearization of Regge calculus. *Numerische Mathematik* 119, 4 (2011), 613–640.
- [17] CIARLET, P. An introduction to differential geometry with applications to elasticity. *Journal of Elasticity* 78-79, 1-3 (2005), 1–207.
- [18] DZIUK, G., AND ELLIOTT, C. M. Finite element methods for surface pdes. *Acta Numerica* 22 (2013), 289–396.
- [19] GERDES, K., MATACHE, A., AND SCHWAB, C. Analysis of membrane locking in hp FEM for a cylindrical shell. *ZAMM - Journal of Applied Mathematics and Mechanics / Zeitschrift für Angewandte Mathematik und Mechanik* 78, 10 (1998), 663–686.
- [20] HAKULA, H., LEINO, Y., AND PITKRANTA, J. Scale resolution, locking, and high-order finite element modelling of shells. *Computer Methods in Applied Mechanics and Engineering* 133, 3 (1996), 157 – 182.
- [21] HAURET, P., AND HECHT, F. A discrete differential sequence for elasticity based upon continuous displacements. *SIAM Journal on Scientific Computing* 35, 1 (2013), B291–B314.

- [22] HIPTMAIR, R. Canonical construction of finite elements. *Mathematics of Computation of the American Mathematical Society* 68, 228 (1999), 1325–1346.
- [23] KOSCHNICK, F., BISCHOFF, M., CAMPRUBÍ, N., AND BLETZINGER, K.-U. The discrete strain gap method and membrane locking. *Computer Methods in Applied Mechanics and Engineering* 194, 21-24 (2005), 2444–2463.
- [24] LI, L. *Regge Finite Elements with Applications in Solid Mechanics and Relativity*. PhD thesis, University of Minnesota, 2018.
- [25] NÉDÉLEC, J. C. Mixed finite elements in r3. *Numerische Mathematik* 35, 3 (1980), 315–341.
- [26] NÉDÉLEC, J. C. A new family of mixed finite elements in R3. *Numerische Mathematik* 50, 1 (1986), 57–81.
- [27] NEUNTEUFEL, M., AND SCHÖBERL, J. The Hellan–Herrmann–Johnson method for nonlinear shells. <https://arxiv.org/abs/1904.04714> (2019).
- [28] PECHSTEIN, A., AND SCHÖBERL, J. The TDNNS method for Reissner–Mindlin plates. *Numerische Mathematik* 137, 3 (2017), 713–740.
- [29] PITKÄRANTA, J. The problem of membrane locking in finite element analysis of cylindrical shells. *Numerische Mathematik* 61, 1 (1992), 523–542.
- [30] PITKÄRANTA, J., LEINO, Y., OVASKAINEN, O., AND PIILA, J. Shell deformation states and the finite element method: A benchmark study of cylindrical shells. *Computer Methods in Applied Mechanics and Engineering* 128, 1 (1995), 81 – 121.
- [31] RAVIART, P. A., AND THOMAS, J. M. *A mixed finite element method for 2-nd order elliptic problems*. Springer Berlin Heidelberg, Berlin, Heidelberg, 1977, pp. 292–315.
- [32] REGGE, T. General relativity without coordinates. *Il Nuovo Cimento (1955-1965)* 19, 3 (Feb 1961), 558–571.
- [33] SCHÖBERL, J. NETGEN an advancing front 2d/3d-mesh generator based on abstract rules. *Computing and Visualization in Science* 1, 1 (1997), 41–52.
- [34] SCHÖBERL, J. C++11 implementation of finite elements in NGSolve. *Institute for Analysis and Scientific Computing, Vienna University of Technology* (2014).
- [35] SINWEL, A., AND SCHÖBERL, J. Tangential-displacement and normal-normal-stress continuous mixed finite elements for elasticity. *Math. Models Methods Appl. Sci.* 21, 8 (2011), 1761–1782.
- [36] STOLARSKI, H., AND BELYTSCHKO, T. Membrane locking and reduced integration for curved elements. *Journal of Applied Mechanics* 49, 1 (1982), 172–176.
- [37] STOLARSKI, H., AND BELYTSCHKO, T. Shear and membrane locking in curved C0 elements. *Computer methods in applied mechanics and engineering* 41, 3 (1983), 279–296.
- [38] SURI, M. Analytical and computational assessment of locking in the hp finite element method. *Computer methods in applied mechanics and engineering* 133, 3-4 (1996), 347–371.
- [39] WHITNEY, H. *Geometric integration theory*. Princeton University Press, Princeton, N. J, 1957.
- [40] WILLIAMS, R. M., AND TUCKEY, P. A. Regge calculus: a brief review and bibliography. *Classical and Quantum Gravity* 9, 5 (1992), 1409.
- [41] ZAGLMAYR, S. *High Order Finite Element Methods for Electromagnetic Field Computation*. PhD thesis, Johannes Kepler Universität Linz, 2006.

- [42] ZIENKIEWICZ, O., AND TAYLOR, R. *The Finite Element Method. Vol. 1: The Basis*, 5th ed. Butterworth-Heinemann, Oxford, 2000.
- [43] ZIENKIEWICZ, O. C., TAYLOR, R. L., AND TOO, J. M. Reduced integration technique in general analysis of plates and shells. *International Journal for Numerical Methods in Engineering* 3, 2 (1971), 275–290.